Pharmaceutical Research, Vol. 25, No. 7, July 2008 (© 2008)
DOI: 10.1007/s11095-008-9554-y

Research Paper

Dissolution Enhancement by Bio-Inspired Mesocrystals: The Study of Racemic (*R*,*S*)-(±)-Sodium Ibuprofen Dihydrate

Tu Lee[1,2,3] and Chyong Wen Zhang[1]

Received August 16, 2007; accepted February 4, 2008; published online February 27, 2008

Purpose. The aim of this paper is to enhance the dissolution rate of racemic (*R*,*S*)-(±)-sodium ibuprofen dihydrate via a bio-inspired method of growing mesocrystals.
Materials and Methods. Mesocrystals of racemic (*R*,*S*)-(±)-sodium ibuprofen dihydrate were successfully prepared from a supersaturated aqueous solution of racemic (*R*,*S*)-(±)-sodium ibuprofen dihydrate having the initial degree of supersaturation, S_0, of 1.326 and the initial saturated concentration, C^*, of 0.986 mol/l at 25°C with sodium dodecyl sulfate (SDS) at a concentration of 0.10 g/l. Dynamic light scattering, scanning electron microscopy, powder X-ray diffraction, differential scanning calorimetry, and optical microscopy with cross polarizers were employed to understand the formation mechanism and to characterize the superstructures of the SDS generated mesocrystals.
Results. The SDS generated mesocrystals were the assembly of the oriented attachment of racemic (*R*,*S*)-(±)-sodium ibuprofen dihydrate nano-sized platelets under the mediation of the side-to-side interaction between SDS and racemic (*R*,*S*)-(±)-sodium ibuprofen dihydrate. The SDS generated mesocrystals contained a mixture of the racemic compounds in α- and β-forms and the resolved racemic conglomerate in γ-form with no detectable amount of SDS. The dissolution rate of the SDS generated mesocrystals was more rapid than the one of its counterpart made by conventional crystallization pathway.
Conclusions. The crystallization of racemic (*R*,*S*)-(±)-sodium ibuprofen dihydrate in the presence of SDS yielded well-faceted, well-separated, but almost perfectly three-dimensionally aligned nano-sized platelets. This kind of bio-inspired mesocrystal superstructure has definitely opened a new doorway for crystal engineering and pre-formulation design in pharmaceutical industry. The future work is to study the mesocrystal formation of some other active pharmaceutical ingredients in organic solvent systems and to develop an efficient method for screening the additives.

KEY WORDS: birefringence; dissolution rate; mesocrystals; racemic (*R*,*S*)-(±)-sodium ibuprofen dihydrate; sodium dodecyl sulfate.

INTRODUCTION

The number of active pharmaceutical ingredients (APIs) has increased dramatically every year (1). It is because the *in vivo* animal screens have been largely replaced by the *in vitro* assays, combinatorial chemistry, and application of genomics to discover the most potent lead compounds (2). At the same time, blockbuster drugs representing 50% to 60% of pharmaceutical sales are coming off patent within the next few years (3). Therefore, improving the dissolution rate of the solid dosage forms and re-designing the dissolution characteristics of the current drug products to extend the products' life are in high demand.

There are several ways for optimizing drug delivery, such as preparing salt forms of ionizable compounds (4,5), using an amorphous phase (6), switching over to a different polymorph (7–10), utilizing co-crystal formers (CCFs) (2,11–15), and resorting to crystal size reduction to the nanometer-sized range by nanotechnology (16–21). After all, all of these methods are focusing on the manipulation of the intermolecular interactions from the angstrom level to the self-assembled, long-range order of API molecules at the nanometer length scale in the solid state. And yet, none of this method has addressed on the materials synthesis and spatial control over "all" length scales (22,23), extending from the angstrom level all the way up to the micron level by self-assembly as vividly illustrated by the mesocrystal formation mechanism in bio-inspired mineralization (24–26). The working principle of bio-inspired mineralization relies heavily on the self-organization of the pre-formed and polymorph-specific primary particles to an ordered superstructure by an oriented attachment which may then be fused into a single

[1] Department of Chemical and Materials Engineering, National Central University, 300 Jhong-Da Rd, Jhong-Li City 320, Taiwan, Republic of China.
[2] Institute of Materials Science and Engineering, National Central University, 300 Jhong-Da Rd, Jhong-Li City 320, Taiwan, Republic of China.
[3] To whom correspondence should be addressed. (e-mail: tulee@cc.ncu.edu.tw)

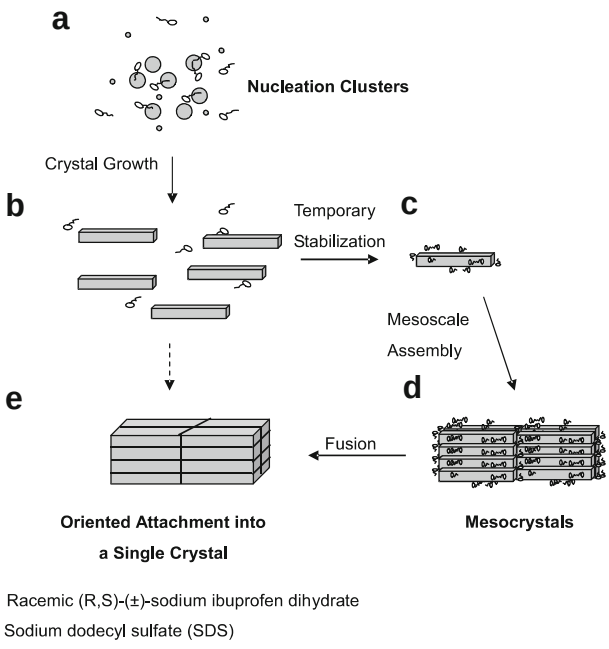

Fig. 1. Schematic representation of mesocrystal formation. **a** Nucleation clusters form in the presence of SDS and grow until they reach the size of the critical crystal nucleus growing to **b** primary nanometer-sized platelets. SDS molecules are adsorbed onto the primary nanometer-sized platelets before they undergo a mesoscale assembly to form **c** a mesocrystal. The building units of the mesocrystal can crystallographically fuse to form **d** a single-crystal-like oriented attachment.

crystal (24) under the guidance of the increasing Hamaker constant (27,28) (Fig. 1).

Although the productions and characterizations of mesocrystals have already been demonstrated on many inorganic compounds (24–26), studies on the formation of mesocrystals of organic molecules and clear demonstrations on the end use of them are rare (23,27,29,30). Therefore, the aim of this paper is to promote the concept of making API mesocrystals according to the scheme in Fig. 1 as a new means for specifically enhancing the dissolution rate of the solid dosage form. The racemic compound (*R*,*S*)-(±)-sodium 2-(4-isobutylphenyl) propionate dihydrate or (*R*,*S*)-(±)-sodium ibuprofen dihydrate (Fig. 2a) was chosen as the model API in this work to test out the concept, because (1) its parent acid (R/S)-(±)-ibuprofen has worldwide commercial values in analgesic, anti-inflammatory, and antipyretic therapies (31), (2) we are familiar with this compound (32), (3) it is a chiral molecule (33), (4) it can be crystallized into α, β, and γ polymorphs depending on the processing conditions (34), (5) its electrical conductance in aqueous solution allows the simple use of an electrical conductivity meter to monitor the nucleation phase in the crystallization event and the dissolution behavior of the derived mesocrystals, and finally, (6) its inherent high aqueous solubility can be used to challenge the dissolution characteristics of the derived mesocrystals.

The mesocrystals of racemic (*R*,*S*)-(±)-sodium ibuprofen dihydrate stacked with nanocrystalline platelets were obtained when using sodium dodecyl sulfate (SDS) as an additive (Fig. 2b). SDS, also known as sodium lauryl sulfate (SLS), is a common anionic surfactant widely used in household products, pharmaceutical formulations (35), and the growth of nanotubes and nanowires (36). The concentration of SDS in our study was kept at only 0.1 g/l in an aqueous solution. This concentration was typically fallen in a reasonable range as compared with other systems (37), well below the human lethal oral dose of 0.5 to 5 g/kg in water (35), and different from the usual high weight fractions of additives in the solid dispersion technology (16,17,19).

Scanning electron microscopy (SEM) was used to observe the architecture of mesocrystals. The energy-dispersive spectrometry (EDS) was utilized for the detection of the presence of residual SDS in the mesocrystals based on the qualitative analysis of sulfur originated from SDS. Powder X-ray diffraction (PXRD) was performed to examine the time-evolving crystallite alignment and the crystallite size in the mesocrystals. Optical microscopy with crossed polarizers was used to show the interference colors related to birefringence of the three-dimensional mesocrystal anisotropic alignment. Dynamic light scattering was utilized to measure the particle size distribution in the beginning of the crystallization event. Differential scanning calorimetry (DSC) was employed to identify traces of SDS and the polymorphism of racemic (*R*,*S*)-(±)-sodium ibuprofen dihydrate. Hexadecyltrimethyl ammonium bromide (HTMAB; Fig. 2c), a cationic surfactant, was employed to replace SDS as a probing additive in some experiments for revealing the intermolecular interaction orientations between the molecules of SDS and racemic (*R*,*S*)-(±)-sodium ibuprofen dihydrate. Finally, dissolution tests were carried out by measuring the concentration of dissolved mesocrystals of racemic (*R*,*S*)-(±)-sodium ibuprofen dihydrate versus time with the use of an electrical conductivity meter.

MATERIALS AND METHODS

Chemical Reagents

All chemical reagents were purchased from Sigma-Aldrich Corporation (St. Louis, MO, USA). Anhydrous

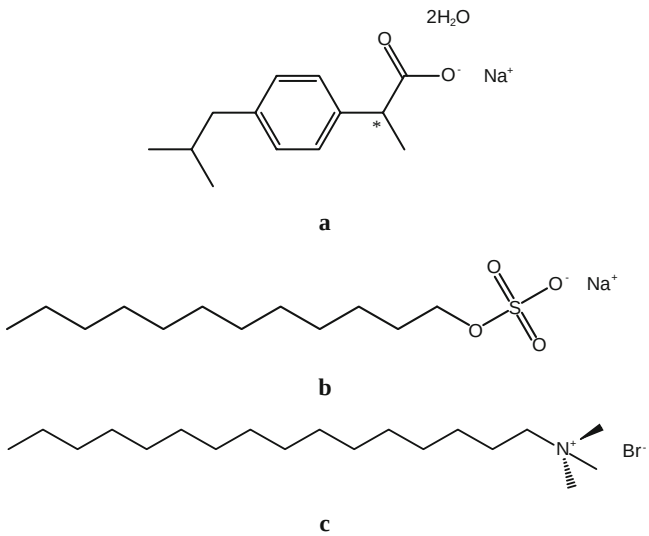

Fig. 2. Molecular structures of **a** racemic (*R*,*S*)-(±)-sodium ibuprofen dihydrate, **b** sodium dodecyl sulfate, and **c** hexadecyltrimethyl ammonium bromide.

ibuprofen sodium salt ($C_{13}H_{17}NaO_2$, molecular weight of 228.29 g/mol, batch number of 027K2111) turned into a dihydrate of racemic (*R*,*S*)-(±)-sodium 2-(4-isobutylphenyl) propionate (racemic (*R*,*S*)-(±)-sodium ibuprofen dihydrate) with a molecular formula of $C_{13}H_{17}NaO_2{\cdot}2H_2O$ and a molecular weight of 264.29 g/mol when it was placed in air for about a week (32). The two additives used were sodium dodecyl sulfate (SDS; $NaC_{12}H_{25}SO_4$, molecular weight of 288.38 g/mol, purity 98%, batch number of S21318-514) and hexadecyltrimethyl ammonium bromide ($C_{19}H_{42}NBr$, molecular weight of 364.46 g/mol, purity 99%, batch number of 076K0109). Acetone (CH_3COCH_3, molecular weight of 58.08 g/mol, HPLC-Spectro grade 99.5%, boiling point of 56°C, lot number of 411050) was used for rinsing the filter cake of racemic (*R*,*S*)-(±)-sodium ibuprofen dihydrate. Reversible osmosis (RO) water was clarified with a water-purification system (Milli-RO Plus, Millipore, Billerica, MA, USA) and used throughout all experiments.

Experimental

A supersaturated aqueous solution of racemic (*R*,*S*)-(±)-sodium ibuprofen dihydrate at 25°C was prepared by dissolving about 4.49 g of racemic (*R*,*S*)-(±)-sodium ibuprofen dihydrate completely at 30°C in a 25 ml scintillating vial filled with 13 ml of water with and without SDS at a concentration of 0.10 g/l or HTMAB at a concentration of 0.13 g/l. The temperature was then raised to 40°C and kept at that temperature for 30 min upon stirring at 250 rpm in order to destroy all invisible nuclei. The unsaturated solution at 40°C would become supersaturated instantly when the vial was immersed in a water bath at 25°C. The degree of this initial supersaturation, S_0, was calculated to be 1.326 with an initial saturated concentration, C^*, of 0.986 mol/l which was equivalent to the solubility of 261 mg/ml at 25°C in an aqueous solution. The relatively high supersaturation was the driving force for the spontaneous nucleation which led to a large number of nanometer-sized crystals in the beginning of the crystallization event. Crystals of racemic (*R*,*S*)-(±)-sodium ibuprofen dihydrate grown with and without SDS were harvested in 30 min and 1 h into the course of crystallization after the first crystal was visible. The crystals were filtered, rinsed with acetone, and oven dried at 40°C for 4 h. Although dehydration would not occur in the ambient condition (32), all crystals were freshly prepared and stored in an ambient condition for no more than two days to minimize the possible fusion of oriented nanoparticle subunits of SDS generated mesocrystals. Each experiment was repeated at least three times to generate 2.5 g of crystalline solids for every dissolution trial.

Analytical Instrumentations

Electrical Conductivity

An electrical conductivity meter (CONSORT K611, Conductivity Instruments, Turnhout, Belgium) was used to monitor the induction period of crystallization at 25°C and the conductivity of the aqueous solution of racemic (*R*,*S*)-(±)-sodium ibuprofen dihydrate in the dissolution tester at 37.5°C as a function of time. If necessary, the conductivity was converted into the corresponding concentration based on two pre-determined calibration curves, one at 25°C and the other at 37.5°C of various concentrations of aqueous solutions of racemic (*R*,*S*)-(±)-sodium ibuprofen dihydrate without SDS. This approximation was acceptable because the concentration of racemic (*R*,*S*)-(±)- sodium ibuprofen dihydrate was much higher than the one of SDS at all times. The instrument was calibrated with 0.01 M of KCl each time before use with an extrapolated conductivity of 1,413 μS at 25°C.

Dynamic Light Scattering (DLS)

The particle size distribution of (*R*,*S*)-(±)-sodium ibuprofen dihydrate in the beginning of the crystallization event was measured by Malvern Zetasizer Nano (Malvern, Worcestershire, UK) with a He–Ne laser source of 4 mW and 633 nm. The refractive index and the absorption coefficient of (*R*,*S*)-(±)-sodium ibuprofen dihydrate were estimated to be 1.5 and 0.033 respectively based on the averaged values of most organic substances. About 1 ml of an aqueous solution of (*R*,*S*)-(±)-sodium ibuprofen dihydrate solution with an initial supersaturation, S_0, of 1.326 was introduced in a low-volume disposable cuvette.

Scanning Electron Microscopy (SEM)

A scanning electron microscope (SEM) (Hitachi S-3500N, Tokyo, Japan) was used to observe the morphology of all sample crystals of racemic (*R*,*S*)-(±)-sodium ibuprofen dihydrate. Both secondary electron imaging (SEI) and back-scattered electron imaging (BEI) emitted by or transmitted through the bombarded sample surface were collected by the SEM detector. The magnification of the SEM images were 15 to 300,000-fold. The operating pressure and the voltage were at 10^{-5} Pa and 15.0 kV respectively. All samples were mounted on a piece of carbon conductive tape (Prod. No. 16073, TED Pella Inc., California, USA) and then sputter-coated with gold (Hitachi E-1010 Ion Sputter, Tokyo, Japan) with a thickness of about 6 nm. The discharge current used for the ion sputter was about 0 to 30 mA and the vacuum was around 10 Pa. The X-ray emitted by the interaction of electrons with the sample specimen was collected in the SEM by the energy-dispersive spectrometer (EDS; Noran Vantage DI, Thermo Scientific, Massachusetts, USA) which was designed to distinguish deferent levels of X-ray energy. The EDS spectroscopy was used for the sulfur analysis originated from SDS.

Powder X-Ray Diffraction (PXRD)

Powder X-ray diffraction was employed on a powder X-ray diffractometer (Bruker D8 Advance, Karlsruhe, Germany). The source of PXRD was CuKα radiation (λ= 1.542 Å) and the diffractometer was operated at 40 kV and 41 mA. The X-ray was passed through a 1 mm incident slit and the signal was passed through a 1 mm detector slit, a nickel filter, and another 0.1 mm detector slit. The detector type was a scintillation counter. The scanning rate was 1.2° 2θ/min with a chopper increment of 0.02° 2θ. The angular range was from 5° to 35° 2θ under room temperature. The quantity of sample used was around 20 to 30 mg.

Differential Scanning Calorimetry (DSC)

Thermal analytical data of 3 to 5 mg of sample crystals of racemic (*R*,*S*)-(±)-sodium ibuprofen dihydrate placed in perforated, aluminum 60-μl pans, were collected on a Perkin Elmer DSC-7 calorimeter (Perkin Elmer Instruments LLC, Shelton, CT, USA) with a heating rate of 10°C/min from 50°C to 200°C using nitrogen 99.990% as a blanket gas. The temperature axis was calibrated with indium 99.999% (Perkin Elmer Instruments LLC, Shelton, CT, USA).

Optical Microscopy (OM)

The interference colors caused by birefringence of all sample crystals of racemic (*R*,*S*)-(±)-sodium ibuprofen dihydrate was examined by an Olympus BX51 Microscope (Olympus, Tokyo, Japan) equipped with an Olympus U-PO3 polarizer (Olympus, Tokyo, Japan), a MotiCam 2000 2.0 Megapixel CCD camera (Motic China Group Co. Ltd., Xiamen, People's Republic of China) and a Motic Images Plus 2.0 ML digital camera software.

Dissolution

A dissolution test station (SR6, Hanson Research Corporation, Chatsworth, CA, USA) Type II (paddle method) at rotation speed of 50 rpm was used for *in vitro* testing. Dissolution tests of all sample crystals of racemic (*R*,*S*)-(±)-sodium ibuprofen dihydrate were carried out on a 2.5-g base of 250- to 350-μm sieve fraction cut. RO water with pH of 6.0 was used as the dissolution medium. The volume and temperature of the dissolution medium were 900 ml and 37.5±0.2°C respectively (38). The real-time concentration of the dissolved racemic (*R*,*S*)-(±)-sodium ibuprofen dihydrate was monitored by the electrical conductivity meter. The dissolution measurements were repeated three times over the full course to obtain mean values and standard deviations for each time point.

RESULTS AND DISCUSSION

The induction period was the time interval measured between the moment at which the supersaturated aqueous solution of racemic (*R*,*S*)-(±)-sodium ibuprofen dihydrate with and without SDS had just reached 25°C with an initial concentration, C_0, of 1.31 mol/l or 1.31 M ($C_0 = S_0 \times C^* = 1.326 \times 0.986$ mol/l) and the time point at which the conductivity of the mother liquor began to drop (i.e. the turning point). The induction period was determined to be 19.4±5.4 and 15.6±5.4 min with and without SDS respectively from the three separate measurements of electrical conductivity against time. The conductivity was converted into the concentration of racemic (*R*,*S*)-(±)-sodium ibuprofen dihydrate in an aqueous solution by a pre-determined calibration curve established at 25°C. The three corresponding concentration-versus-time curves (i.e. de-supersaturation curves) were plotted in Fig. 3.

The poor reproducibility of the induction period could be due to the self-association property (39) of the amphiphilic racemic (*R*,*S*)-(±)- sodium ibuprofen dihydrate molecules because of the initial concentration in the system of C_0=

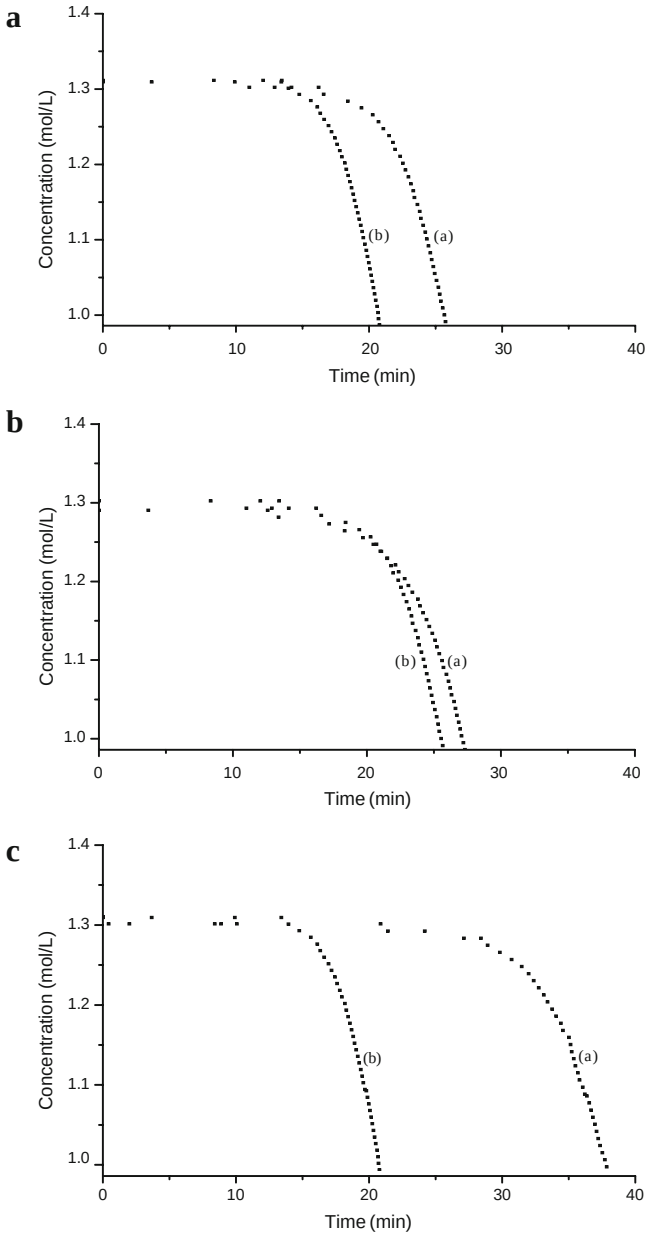

Fig. 3. Three separate repeating trials (**a**–**c**) of the de-supersaturation curve of racemic (*R*,*S*)-(±)-sodium ibuprofen dihydrate at S_0=1.326 and C^*=0.986 mol/l in an aqueous solution at 25°C (a) with and (b) without sodium dodecyl sulfate of 0.10 g/l.

1.31 M at 25°C which was higher than the critical micelle concentration (CMC) of racemic (*R*,*S*)-(±)- sodium ibuprofen dihydrate of 0.18 M at 25°C (40). We speculated that the self-association process into micelles could be competing with the nucleation step in crystallization. Therefore, the processing history, the controlled environments of the solution and the local fluctuation in concentration were crucial to the microstructure of this particular complex fluid.

The conductivity meter measured the conductivity of only the dissolved sodium ibuprofen solutes. Therefore, the conductivity could reveal the induction period as the sum of the time needed for the supersaturation reaching the steady-state of the primary nucleation (Fig. 1a), the time of primary

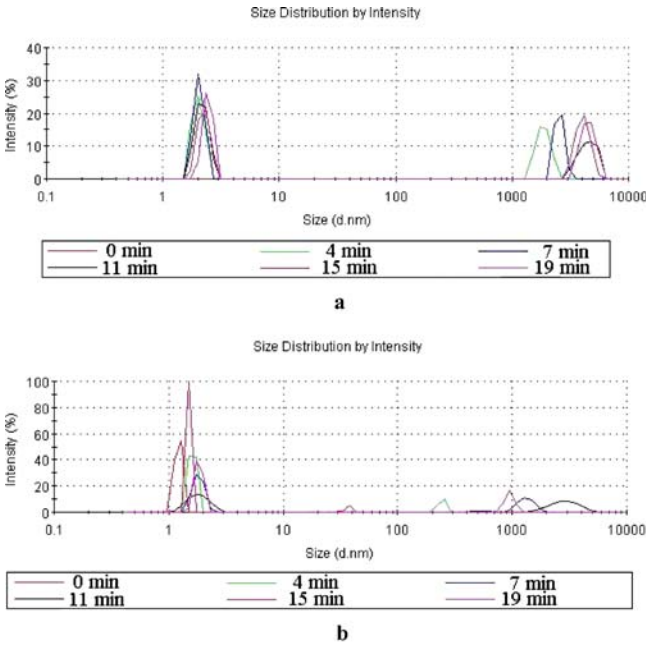

Fig. 4. Particle size distribution as a function of time by dynamic light scattering of racemic (*R*,*S*)-(±)-sodium ibuprofen dihydrate at S_0= 1.326 and C^*=0.986 mol/l in an aqueous solution at 25°C (**a**) with, and (**b**) without sodium dodecyl sulfate of 0.10 g/l.

nucleation, and the time required for the critical nucleus to grow to a crystallite size which caused the solution to be de-supersaturated to a level detectable by the inherent sensitivity of the conductivity meter (Fig. 1b). The presence of SDS in the supersaturated aqueous solution filled with clusters of racemic (*R*,*S*)-(±)-sodium ibuprofen dihydrate of different sizes had increased the induction period because the configurationally similar SDS could have been incorporated to the nuclei of racemic (*R*,*S*)-(±)-sodium ibuprofen dihydrate to raise the Gibbs free energy barrier of forming clusters of a critical size through the increase of the solution–solid interfacial energy of the clusters of racemic (*R*,*S*)-(±)-sodium ibuprofen dihydrate. This suggested that the bonding structure of the clusters of racemic (*R*,*S*)-(±)-sodium ibuprofen dihydrate in the presence of SDS was very different to the liquid structure of the solution than to the ones in the absence of SDS. In other words, the presence of SDS might have made the micelles more stable and delayed the homogeneous nucleation. However, the conductivity measurement versus time had become unreliable during the latter period of crystal growth due to poor mixing (Fig. 3). The texture of the solution had turned from a fluid into a slurry as the population number of crystals began to increase when the supersaturated aqueous solution was being de-supersaturated.

But to verify the formation and the existence of primary particles within the induction period in the beginning of the crystallization event, DLS was employed to examine the sodium ibuprofen dihydrate systems with and without SDS. Intriguingly, the sodium ibuprofen dihydrate system with SDS exhibited a bimodal distribution (Fig. 4a). A set of sharp distribution peaks at 2 nm, which neither got shifted nor broaden with time, implied the self-association of the amphiphilic racemic (*R*,*S*)-(±)-sodium ibuprofen dihydrate molecules into spherical micelles with a radius of 1 nm. It was about the length of the amphiphilic sodium ibuprofen dihydrate molecule. The large gap between the first peak at 2 nm and the second peak around 1,500 nm at the fourth min in Fig. 4a further suggested that the 2-nm sized spherical micelles might well be the nucleation clusters with the critical radius, r_c, of 2 nm. A massive, one-step assembly of 2-nm sized aggregates (i.e. micelles or nucleation clusters; Fig. 1c) then gave rise to a size distribution of primary particles (which might well be aggre-

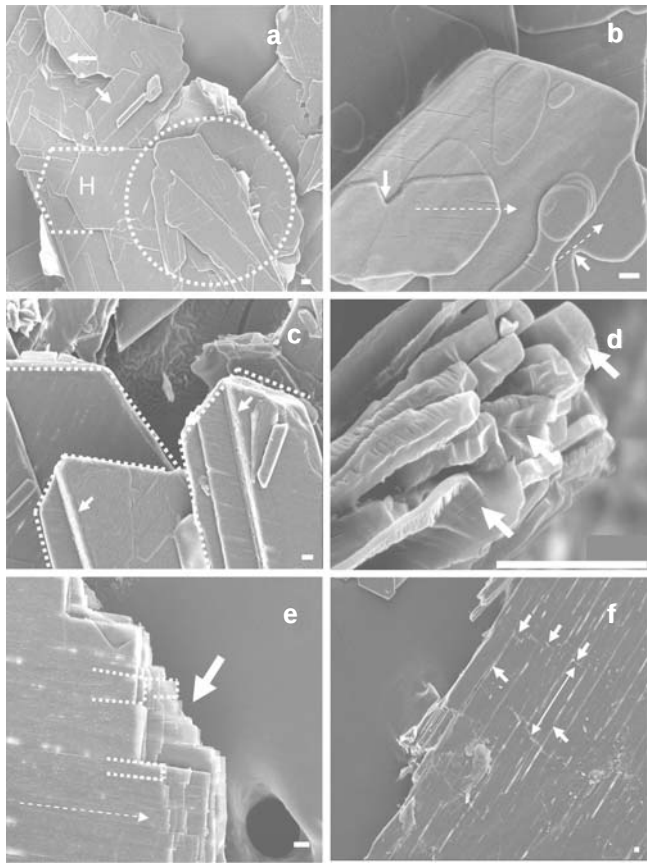

Fig. 5. SEM images of racemic (*R*,*S*)-(±)-sodium ibuprofen dihydrate crystals: **a** grown without SDS and harvested 1 h into the course of crystallization. A thin and flat hexagonal platelet (*H*) was located beneath an aggregate of irregular-shaped platelets (*circled by white dots*). Islands (pointed by *white arrows*) were formed on crystal faces due to the two-dimensional nucleation. **b** Grown with SDS and harvested 1 h into the course of crystallization. The edges of the platelets were deformed, curved and irregular. The V-grooves were formed (indicated by *white arrows*). The elongated pores generated by the water removal were running across the platelets in the [100] directions (indicated by *white dashed arrows*). **c** Under the mediation of SDS, the platelets were grown large in size (laced by the *white dashed lines*) and wide in thickness (pointed by the white arrows). **d** Well-faceted fracture surface of a mesocrystal filled with nano-sized thick layered platelets (pointed by the *white arrows*). **e** The oriented assembly of well-separated, nano-sized rectangular platelets (laced by the *white dashed lines*) were aligned in the [100] direction (indicated by the *white dashed line*), and **f** all nano-sized platelets were narrow in size distribution (indicated by the *white double head arrows*) and well-assembled into a single-crystal-like deck structure (indicated by the *white arrows*). Scale bar=10 μm.

gates) around 1,500 nm which then assembled into mesocrystals of size distributions larger than 1,500 nm. The second peak gradually got shifted away from 1,500 nm to the right as the mesocrystals started to grow as a function of time. The relatively constant height and width of the first peak at 2-nm as time went by pointed to the fact that the birth rate of primary nucleation of the 2-nm aggregates was constantly balanced out by the rate of formation of mesocrystals.

On the other hand, the DLS of the sodium ibuprofen dihydrate system without SDS displayed the first peak around 1.1 to 2 nm and a shift of the second peak from 40, to 250, to 1,500 and even up to 3,000 nm as time increased (Fig. 4b). Although the self-association of the amphiphilic racemic (*R*, *S*)-(±)- sodium ibuprofen dihydrate molecules into spherical micelles and nucleation clusters still took place, a massive, one-step assembly of 2-nm sized aggregates into 1,500 nm-size ranged aggregates was not observed in the absence of SDS. Seemingly, the crystal growth followed a slower, step-by-step conventional mechanism of 4 steps: (1) homogeneous nucleation, (2) nucleation cluster growth, (3) aggregation growth, and (4) secondary nucleation.

SEM revealed that as soon as the clusters of racemic (*R*, *S*)-(±)-sodium ibuprofen dihydrate larger than the critical size were formed in a supersaturated solution without SDS, they began to grow into thin but flat crystalline platelets with a definitive hexagonal geometry (Fig. 5a) most likely under the guidance of hydrogen bondings between the carboxylate head groups in the axial [001] direction of the molecule and the π-π interactions between the aromatic rings in the lateral [100] direction of the molecule (32). As the crystal face grew larger, a two-dimensional nucleus was created on the (010) face surface by an epitaxial matching (32). Once the surface nucleus was born, it spread across the surface to produce another layer of island (Fig. 5a). As the number of crystals started to increase, some of the crystals with different sizes began to aggregate as well (Fig. 5a).

But with the presence of SDS, the mesocrystals once formed in the induction period (second peak at 1,500 nm in Fig. 4a) might continue to grow through the assembly with another mesocrystals under the guidance of SDS, and eventually fused into an oriented attachment which was verified by SEM, PXRD and OM.

The hypothesis that the crystal faces were covered with adsorbed SDS molecules in an aqueous environment was fully supported by the interference of SDS on the crystal growth kinetics (41). Fig. 5b clearly illustrated the deformed crystal habit. The edges of racemic (*R*,*S*)-(±)-sodium ibuprofen dihydrate platelets were no longer straight as in Fig. 5a. On the contrary, they were curved and irregular (Fig. 5b). The platelet surface was also cambered instead of being flat (Fig. 5b). However, EDS indicated that no detectable trace amount of SDS was either inside or outside the crystals. This suggested that SDS was completely removed by rinsing during crystal filtration.

The same morphological effects on the crystal habits of racemic (*R*,*S*)-(±)-sodium ibuprofen dihydrate platelets by replacing SDS with HTMAB had also led us to believe that the alkane tails of SDS and HTMAB, rather than their different charged head groups, had actually played a dominant role in interacting with the crystal faces of racemic (*R*,*S*)-(±)-sodium ibuprofen dihydrate platelets. This type of hydrophobic interaction between SDS and racemic (*R*,*S*)-(±)-sodium ibuprofen dihydrate crystal face probably occurred in a side-to-side fashion due to the large chain volume of SDS (Fig. 1c). This hypothesis was supported substantially

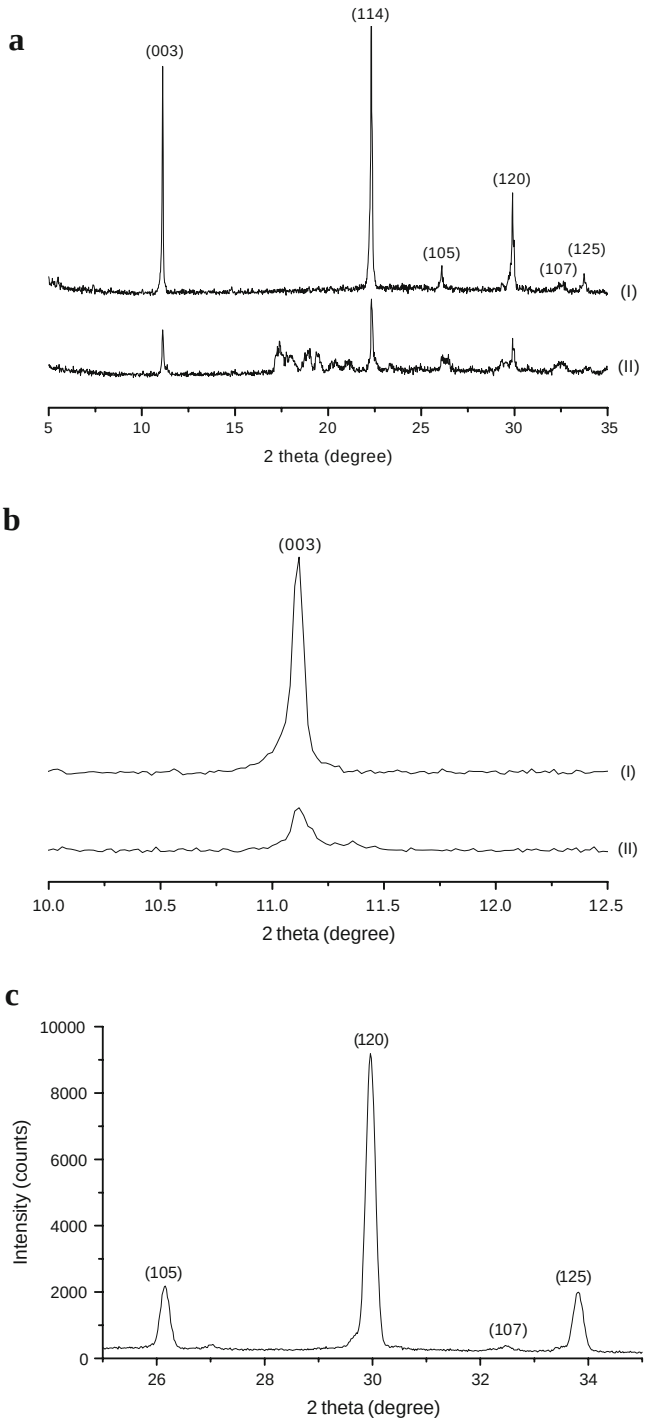

Fig. 6. PXRD patterns of racemic (*R*,*S*)-(±)-sodium ibuprofen dihydrate crystals grown **a** (*I*) at the 30th min into the course of crystallization in the absence of SDS, (*II*) at the 30th min into the course of crystallization in the presence of SDS, **b** the (003) peak of (*I*) at the 30th min into the course of crystallization in the absence of SDS, (*II*) at the 30th min into the course of crystallization in the presence of SDS, and **c** at the first hour into the course of crystallization in the presence of SDS.

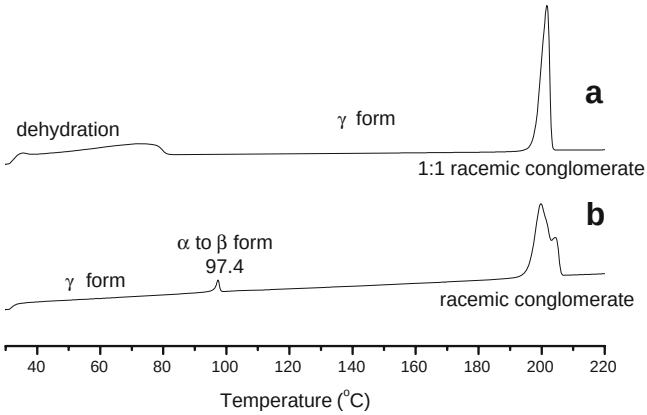

Fig. 7. DSC scans of racemic (*R*,*S*)-(±)-sodium ibuprofen dihydrate crystals grown **a** at the 30th min into the course of crystallization in the absence of SDS, and **b** at the 30th min into the course of crystallization in the presence of SDS.

by the existence of the two V-grooves in Fig. 5b where the hydrophobic interaction between SDS and racemic (*R*,*S*)-(±)-sodium ibuprofen dihydrate happening in the (100) plane inhibited the normal crystal growth in the [100] direction (i.e. the a-axis of the unit cell of racemic (*R*,*S*)-(±)-sodium ibuprofen dihydrate) designated by the elongated pores which were the unzipped locations of the removal of water from the sandwiched layer of (*R*)-(+)-sodium ibuprofen-water-(*S*)-(−)-sodium ibuprofen (32).

The racemic (*R*,*S*)-(±)-sodium ibuprofen dihydrate crystalline platelets grown in the presence of SDS also appeared to be larger and thicker (Fig. 5c) than the ones grown without SDS (Fig. 5a) due to the stacking of ordered platelets (i.e. oriented attachment). When the crystal sample was further broken by using a pair of tweezers, bundles of mesostructure of parallel nano-rectangular platelets was observed by SEM (Fig. 5d). The fracture surface proved that the obtained racemic (*R*,*S*)-(±)-sodium ibuprofen dihydrate crystalline platelet was not a conventional single crystal, or else a flat cleavage plane would have been resulted. The higher magnification of

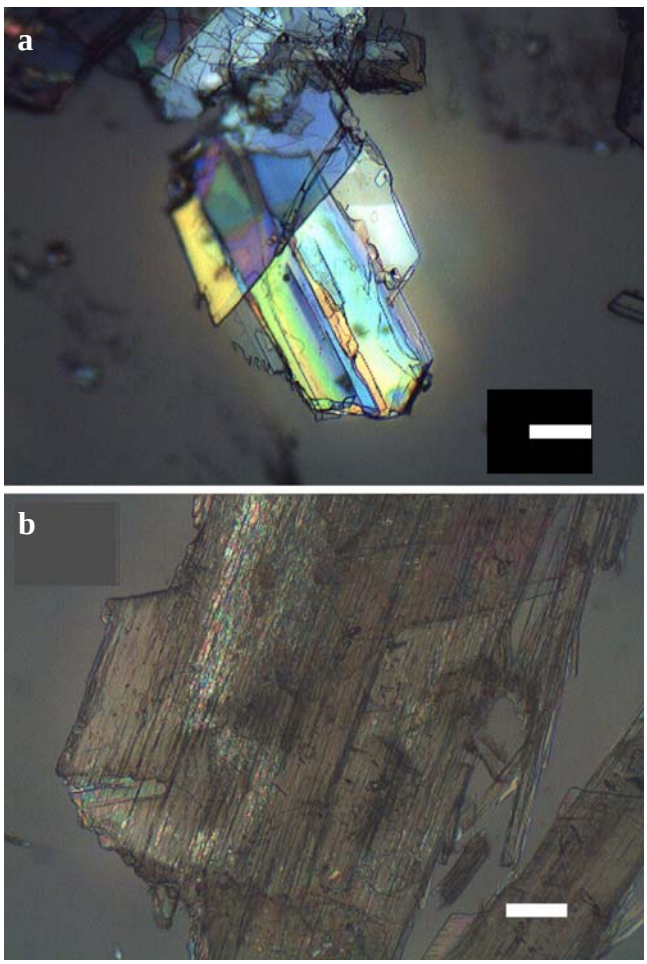

Fig. 8. Optical micrographs of racemic (*R*,*S*)-(±)-sodium ibuprofen dihydrate crystals at the first hour into the course of crystallization **a** with SDS, and **b** without SDS, under the cross polarizers. (scale bar=100 μm).

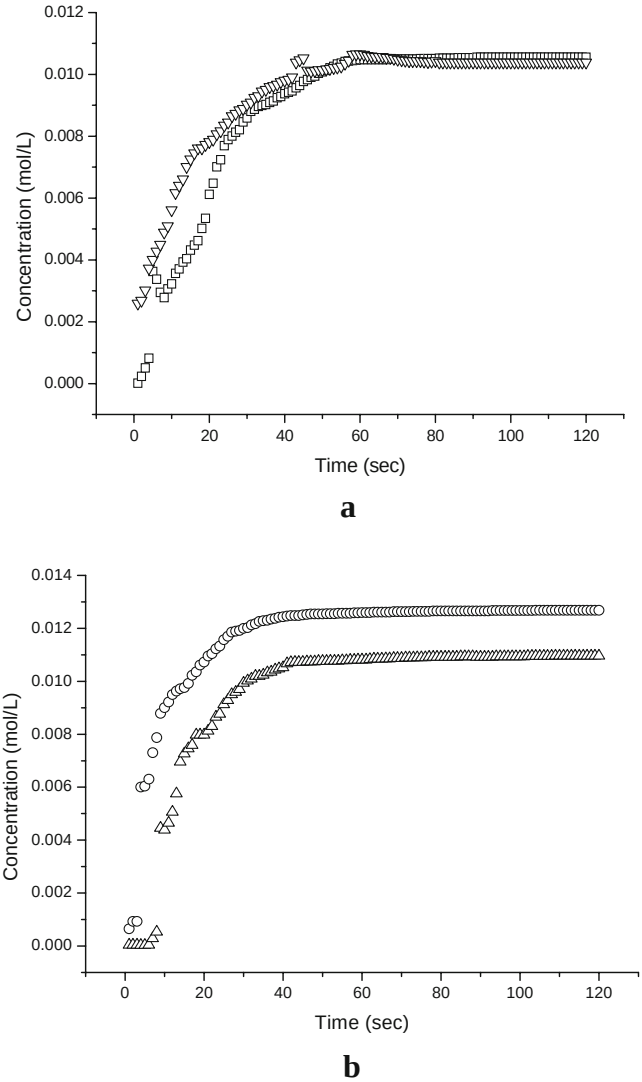

Fig. 9. Dissolution profiles of crystals of racemic (*R*,*S*)-(±)-sodium ibuprofen dihydrate in water at 37.5°C **a** without milling (*inverted triangle*=SDS generated mesocrystals, and *square*=conventional crystals without SDS), and **b** with milling (*circle*=SDS generated mesocrystals, and *triangle*=conventional crystals without SDS).

the faceted face revealed the mesoscale assembly of the nano-rectangular platelets (Fig. 1d) with a narrow size distribution both in width (Fig. 5e) and in length (Fig. 5f) which resembled the aggregates of carbamazepine dihydrate grown under the influence of 5 mg/ml of hydroxypropyl methylcellulose (Methocel K4M) in an aqueous solution after 7 days (29), and DL-alanine crystals formed by crystallization in water with the addition of 1 wt% PEG_{4700}-PEI_{1200}-*S*-*i*BAc (30).

Besides the SEM images, the oriented attachment of the mesocrystals (Fig. 1e) of racemic (*R*,*S*)-(±)-sodium ibuprofen dihydrate was further verified by PXRD and OM. The PXRD patterns of the crystals obtained at the 30th min into the course of crystallization with SDS [Fig. 6a (II)] had peaks with broader width at half maximum than the peaks of the PXRD patterns of the crystals obtained at the 30th min into the course of crystallization without SDS [Fig. 6a (I)]. The average building unit size D in nm was estimated using 2θ in degrees of the (003) peak and its full width at half maximum β in radians by applying the Scherrer formula (42):

$$D = \frac{0.9\lambda}{\beta \cos\theta}$$

where λ of the CuKα radiation source was 0.154 nm. But the PXRD diffractograph of the crystals harvested at the first hour into the course of crystallization with SDS showed well-developed, narrow diffraction peaks with intensities so high that only peaks at 2θ=25° to 35° were collected without causing any damage to the PXRD detector (Fig. 6c). The increase in the intensities of the (105), (120) and (125) peaks in Fig. 6c in comparison to Fig. 6a (II) indicated that the orientational effects of the primary nanocrystalline platelets in the mesocrystal substructure (Fig. 1e) were real whereas the decrease in the intensity of the (107) peak in Fig. 6c in comparison to Fig. 6a (II) suggested that this particular crystal direction might only exist in nanometer dimensions due to very broad peak widths that led to the peak disappearance in the baseline (30).

Racemic (*R*,*S*)-(±)-sodium ibuprofen dihydrate crystals grown from the aqueous solution without SDS demonstrated the typical dehydration endothermic hump around 80°C and a single sharp melting endotherm of γ-Form indicating a 1:1 racemic conglomerate at 200°C (Fig. 7a) (34). However, racemic (*R*,*S*)-(±)-sodium ibuprofen dihydrate crystals harvested from the aqueous solution with SDS displayed an endotherm of α-to-β polymorphic transformation at 97.4°C and a melting endotherm duplet of a resolved γ-Form of racemic conglomerate (Fig. 7b) (34). However, at this stage, we are not sure whether the mesocrystal could contain all the α-, β- and γ-Forms or mesocrystals of the α-, β- and γ-Forms were being existed separately.

The optical micrographs of the mesocrystals harvested at the first hour into the course of crystallization with and without SDS under the crossed polarizers were demonstrated in Fig. 8. As opposed to the conventional crystal, only the SDS generated mesocrystals showed strong interference colors caused by birefringence (Fig. 8a). It was the manifestation of the existence of orientation-dependent differences in refractive index and the existence of the optically anisotropy. This result agreed well with the diffractogram in Fig. 6c where the SDS generated mesocrystals were highly anisotropic and having an oriented attachment.

Finally, the dissolution profiles in Fig. 9a illustrated that the SDS generated mesocrystals did dissolve at a rate (50% drug release time, t_{50}=9.2 s) twice of its counterpart of the conventionally grown crystals (t_{50}=18.8 s). To ensure that this result originated from the intrinsic properties of the SDS generated mesocrystals, and not from the external characteristics of the crystals such as sizes and shapes, dissolution rates of ground SDS generated mesocrystals and ground conventional crystals were also monitored. Grinding was carried out by a mortar and pestle for 30 min. Once again, the dissolution profiles in Fig. 9b showed that the ground SDS generated mesocrystals did dissolve at a rate (50% drug release time, t_{50}=6.0 s) twice of its counterpart of the conventional crystals (t_{50}=12.6 s). Apparently, the higher surface area per unit volume due to the self-organized mesosized platelets, existing in the special hierarchical structure of the SDS generated mesocrystals from the angstrom level to the micron scale provided a larger surface area for enhancing the dissolution.

CONCLUSIONS

The crystallization of racemic (*R*,*S*)-(±)-sodium ibuprofen dihydrate in the presence of SDS yielded well-faceted, well-separated, but almost perfectly three-dimensionally aligned nano-sized platelets. This kind of bio-inspired mesocrystal superstructure has definitely opened a new doorway for crystal engineering and pre-formulation design in pharmaceutical industry. The future work is to study the mesocrystal formation of some other active pharmaceutical ingredients such as acetaminophen and carbamazepine to develop an efficient method for screening the additives.

ACKNOWLEDGEMENTS

This work was supported by a grant from the National Science Council of Taiwan, Republic of China (NSC 95-2113-M-008-012-MY2). Assistance from Ms. Jui-Mei Huang in DSC, Ms. Shew-Jen Weng in PXRD, and Ms. Ching-Tien Lin for SEM and EDS, and all with the Precision Instrument Center and High Valued Instrument Center at National Central University are gratefully acknowledged. We also thank the assistance from Ms. Yi-Yin Lai in DLS with Molecular BioEngineering Laboratory, and my four other students, Mr. Hsiang-Yu Hsieh, Mr. Yeh-Wen Wang, Mr. Hung-Ju Hou, and Mr. Yan-Chan Su in collecting SEM, DLS and dissolution data.

REFERENCES

1. L. J. Sellars. Special report: Executive prophecies—pharmaceuticals in the new millennium. *Pharm. Exec.* 60–72 (January 2002).
2. Ö. Almarsson, and M. J. Zaworotko. Crystal engineering of the composition of pharmaceutical phases. Do pharmaceutical co-crystals represent a new path to improved medicines. *Chem. Commun*. 17:1889–1896 (2004).
3. Trends in the Pharmaceutical Industry. www.patheon.com/overview/trends.html.

4. R. J. Bastin, M. J. Bowker, and B. J. Slater. Salt selection and optimisation procedures for pharmaceutical new chemical entities. *Org. Proc. Res. Dev* **4**(5): 427–435 (2000).
5. S. N. Black, E. A. Collier, R. J. Davey, and R. J. Roberts. Structure, solubility, screening, and synthesis of molecular salts. *J. Pharm. Sci* **96**(5): 1053–1068 (2007).
6. L. R. Hilden, and K. R. Morris. Physics of amorphous solids. *J. Pharm. Sci* **93**(1): 3–12 (2004).
7. R. Hilfiker, J. Berghausen, F. Blatter, A. Burkhard, S. M. PaulDe, B. Freiermuth, A. Geoffroy, U. Hofmeier, C. Marcolli, B. Siebenhaar, M. Szelagiewicz, A. Vit, and M. Raumervon. Polymorphism – Integrated approach from high-throughput screening to crystallization optimization. *J. Therm. Anal. Calor* **73**(2): 429–440 (2003).
8. N. Blagden, and R. J. Davey. Polymorph selection: Challenges for the future? *Cryst. Growth Des* **3**(6):873–885 (2003).
9. T. Lee, S. T. Hung, and C. S. Kuo. Polymorph farming of acetaminophen and sulfathiazole on a chip. *Pharm. Res* **23**(11): 2542–2555 (2006).
10. D. Singhal, and W. Curatolo. Drug polymorphism and dosage form design: A practical perspective. *Adv. Drug Deliv. Rev* **56**(3): 335–347 (2004).
11. P. Vishweshwar, J. A. McMahon, M. L. Peterson, M. B. Hickey, T. R. Shattock, and M. J. Zaworotko. Crystal engineering of pharmaceutical co-crystals from polymorphic active pharmaceutical ingredients. *Chem. Commun.* 36:4601–4603 (2005).
12. S. L. Morissette, Ö. Almarsson, M. L. Peterson, J. F. Remenar, M. J. Read, A. V. Lemmo, S. Ellis, M. J. Cima, and C. R. Gardner. High-throughput crystallization: polymorphs, salts, co-crystals and solvates of pharmaceutical solids. *Adv. Drug Deliv. Rev* **56**(3): 275–300 (2004).
13. H. Koshima, and M. Miyauchi. Polymorphs of a cocrystal with achiral and chiral structures prepared by pseudoseeding: tryptamine/hydrocinnamic acid. *Cryst. Growth Des* **1**(5): 355–357 (2001).
14. G. G. Z. Zhang, R. F. Henry, T. B. Borchardt, and X. Lou. Efficient co-crystal screening using solution-mediated phase transformation. *J. Pharm. Sci* **96**(5): 990–995 (2007).
15. A. M. Thayer. Form and Function. *C&EN*, 17–30 (June 18 2007).
16. A. T. M. Serajuddin. Solid dispersion of poorly water-soluble drugs: early promises, subsequent problems, and recent breakthroughs. *J. Pharm. Sci* **88**(10): 1058–1066 (1999).
17. T. Lee, and J. Lee. Drug-carrier screening on a chip. *Pharm. Tech* **27**(1): 40–48 (2003).
18. J.-F. Chen, M.-Y. Zhou, L. Shao, Y.-Y. Wang, J. Yun, N. Y. K. Chew, and H-K. Chan. Feasibility of preparing nanodrugs by high-gravity reactive precipitation. *Inter. J. Pharm* **269**(1): 267–274 (2004).
19. S. X. Yin, M. Franchini, J. Chen, A. Hsieh, S. Jen, T. Lee, M. Hussain, and R. Smith. Bioavailability enhancement of a COX-2 inhibitor, BMS-347070, from a nanocrystalline dispersion prepared by spray-drying. *J. Pharm. Sci.* **94**(7):1598–1607.
20. N. A. Peppas. Intelligent therapeutics: biomimetic systems and nanotechnology in drug delivery. *Adv. Drug Deliv. Rev* **56**(11): 1529–1531 (2004).
21. P. Van Arnum. Nanotechnology advances in drug delivery. *Pharm. Tech* **31**(6): 48–52 (2007).
22. I. Soten, and G. A. Ozin. New directions in self-assembly: materials synthesis over "all" length scales. *Curr. Opin. Colloid Inter. Sci* **4**(5): 325–337 (1999).
23. Y. Oaki, and H. Imai. Hierarchially organized superstructure emerging from the exquisite association of inorganic crystals, organic polymers, and dyes: a model approach towards supra-biomineral materials. *Adv. Funct. Mater* **15**(9): 1407–1414 (2005).
24. A.-W. Xu, Y. Ma, and H. Cölfen. Biomimetic mineralization. *J. Mater. Chem* **17**(5): 415–449 (2007).
25. H. Cölfen, and M. Antonietti. Mesocrystals: inorganic superstructures made by highly parallel crystallization and controlled alignment. *Angew. Chem. Int. Ed* **44**(35): 5576–5591 (2005).
26. H. Cölfen, and S. Mann. Higher-order organization by mesoscale self-assembly and transformation of hybrid nanostructures. *Angew. Chem. Int. Ed* **42**(20): 2350–2365 (2003).
27. Y. Ma, H. Cölfen, and M. Antonietti. Morphosynthesis of alanine mesocrystals by pH control. *J. Phys. Chem. B* **110**(22): 10822–10828 (2006).
28. C.-M. Chun. Hydrothermal crystallization of barium titanate: mechanisms of nucleation and growth. Ph. D. Dissertation, Department of Geosciences, Princeton University, June 1997.
29. I. Katzhendler, R. Azoury, and M. Friedman. Crystalline properties of carbamazepine in sustained release hydrophilic matrix tablets based on hydroxypropyl methylcellulose. *J. Control. Release* **54**(1): 69–85 (1998).
30. S. Wohlrab, N. Pinna, M. Antonietti, and H. Cölfen. Polymer-induced alignment of DL- alanine nanocrystals to crystalline mesostructures. *Chem. Eur. J* **11**(10): 2903–2913 (2005).
31. B. J. Armitage, J. F. Lampard, and A. Smith. Composition of S-Sodium ibuprofen. US Patent 6,242,000 B1 (2001).
32. T. Lee, Y. H. Chen, and Y. W. Wang. Effects of homochiral molecules of (S)-(+)-ibuprofen and (S)-(-)-sodium ibuprofen dihydrate on the crystallization kinetics of racemic (R,S)-(±)-sodium ibuprofen dihydrate. *Cryst. Growth Des.* **8**(2): 415–426 (2008).
33. Y. Zhang, and D. J. W. Grant. Similarity in structures of racemic and enantiomeric ibuprofen sodium dihydrates. *Acta Cryst.* **C61** (9): m435–m438 (2005).
34. G. G. Z. Zhang, S. Y. L. Paspal, R. Suryanarayanan, and D. J. W. Grant. Racemic species of sodium ibuprofen: characterization and polymorphic relationships. *J. Pharm. Sci* **92**(7): 1356–1366 (2003).
35. S. Behn. Sodium lauryl sulfate. In A. Wade, and P. J. Weller (eds.), *Handbook of Pharmaceutical Excipients*, 2American Pharmaceutical Association, Washington, USA, 1994, pp. 448–450.
36. Y. Xiong, Y. Xie, J. Yang, R. Zhang, C. Wu, and G. Du. *In situ* micelle-template-interface reaction route to CdS nanotubes and nanowires. *J. Mater. Chem* **12**(12): 3712–3716 (2002).
37. N. Jongen, P. Bowen, J. Lemaître, J.-C. Valmalette, and H. Hofmann. Precipitation of Self-organized copper oxalate polycrystalline particles in the presence of hydroxypropylmethylcellulose (HPMC): control of morphology. *J. Colloid Inter. Sci* **226** (2): 189–198 (2000).
38. W. Sorasuchart, J. Wardrop, and J. W. Ayres. Drug release from spray layered and coated drug-containing beads: effects of pH and comparison of different dissolution methods. *Drug Dev. Ind. Pharm* **25**(10): 1093–1098 (1999).
39. A. T. M. Serajuddin. Salt formation to improve drug solubility. *Adv. Drug Deliv. Rev* **59**(7): 603–616 (2007).
40. A. Ridell, H. Evertsson, S. Nilson, and L. Sundelöf. Amphiphilic association of ibuprofen and two nonionic cellulose derivatives in aqueous solution. *J. Pharm. Sci* **88**(11): 1175–1181 (2000).
41. A. L. D. Vries, and T. J. Price. Role of glycopeptides and peptides in inhibition of crystallization of water in polar fishes. *Phil. Trans. R. Soc. Lond. B* **304**(1121): 575–588 (1984).
42. H. P. Klug, and L. E. Alexander. *Crystallite size and lattice strains from line broadening. Chapter 9 in X-ray Diffraction Procedures*, 2nd ed., Wiley, New York, 1974, pp. 657–661.